Direct Observation of Downhill Folding of λ-Repressor in a Microfluidic Mixer

Stephen J. DeCamp,[†] Athi N. Naganathan,[‡] Steven A. Waldauer,[†] Olgica Bakajin,[§] and Lisa J. Lapidus[†*]
[†]Department of Physics and Astronomy, Michigan State University, East Lansing, Michigan; [‡]Department of Protein Science, Centro de Investigaciones Biológicas, Consejo Superior de Investigaciones Cientificas, Madrid, Spain; and [§]Chemistry, Materials, Earth, and Life Sciences Directorate, Lawrence Livermore National Laboratory, Livermore, California

ABSTRACT The protein $\lambda_{6\text{-}85}$ has been implicated in barrierless folding by observations of kinetic relaxation after nanosecond T-jump. In this work we observed folding of this protein after dilution of a high denaturant in an ultrarapid microfluidic mixer at temperatures far below the thermal midpoint. The observations of total intensity and spectral shift of tryptophan fluorescence yielded distinctly different kinetics and activation energies. These results may be explained as diffusion on a low-barrier, one-dimensional, free-energy surface, with different probes having different sensitivities along the reaction coordinate. Additionally, we observed an extremely fast phase within the mixing time that was not observed by T-jump, suggesting that the ensemble of unfolded states populated at high denaturant is distinct from those accessible at high temperature.

INTRODUCTION

One view of protein folding is that it can be described by diffusion on a relatively smooth energy landscape. A classic prediction from this theory of protein folding is the existence of low-barrier or ''downhill'' folding, in which progress to the folded state is not limited by the crossing of one or many distinct and significant free-energy barriers (1,2). Such a protein should fold on the microsecond timescale (3), limited only by the intrinsic rate of diffusion on this landscape, and thus should be observable only by rapid initiation methods, such as T-jump. In recent years, a number of attempts have been made to experimentally observe such folding by searching for fast folders and in some cases engineering mutants for higher thermal stability (4–6). However, such efforts are somewhat hampered by the fact that T-jump usually changes the equilibrium of states significantly only near the thermal melting temperature where the barrier, if any, is largest.

In this work, we observed the folding of a putative downhill folder, λ-repressor, using an ultrarapid mixer capable of diluting denaturant in ~8 μs at temperatures far below the thermal midpoint. Although there is considerable controversy about what kinetic signature a downhill folder should exhibit, there is consensus that different probes may show different kinetic rates if they are sensitive to different structural features on a low-barrier landscape (7). Ma and Gruebele (7) showed that the relaxation rates for a mutant of the λ-repressor differ by a factor of ~3 when measured by tryptophan fluorescence lifetime and infrared absorption spectroscopy. On the other hand, Li et al. (4) observed a ~35 K difference in thermal stability of the protein BBL as measured by fluorescence resonance energy transfer (FRET) and infrared absorption, but very little difference in rates for these two probes at the same temperature. In this work, we observed a significant difference in rates (by a factor of ~10) with different probes, although, surprisingly, these probes were simply the fluorescence intensity change and spectral shift of the same tryptophan in the sequence. However, the quantum yield and emission wavelength are sensitive to different aspects of the local environment of tryptophan, namely, short-range interactions with other side chains and the level of solvation. Therefore, it is reasonable to assume that these probes report on different regions of an energy landscape without large barriers.

The motivation for finding and investigating proteins that fold in a downhill fashion is that the absence of a barrier reveals partially structured, low-population states that localize along the folding reaction coordinate. The two probes employed in this work show that hydrophobic burial occurs significantly before the formation of native contacts near the tryptophan. The future use of other probes, such as FRET or infrared absorption, coupled with low-temperature ultrarapid mixing should reveal the ordering of other native structural elements.

MATERIALS AND METHODS

The plasmids of the three mutants were a kind gift from Martin Gruebele, University of Illinois. The mutations from the wild-type sequence were Y22W A37G A49G (mutant 3), Y22W Q33Y A37G A49G (mutant 4), and D14A Y22W Q33Y G46A G48A (mutant 5). Protein expression and purification were performed according to a previously described protocol (8). The protein was unfolded in 6 M GdnHCl at a concentration of 300 μM and refolded in 100 mM potassium phosphate buffer at pH 7. Folding experiments were conducted with the use of a microfluidic ultrarapid mixer of the type developed by Knight et al. (9) and Hertzog et al. (10,11), and modified by Yao and Bakajin (12). The mixer is made from a 500 μm thick fused silica wafer with channels typically etched 10 μm deep, and a second 170 μm wafer bonded on top to seal the device. All flows are in the laminar regime and the flow rates can be computed from the applied pressures by mathematical simulations (COMSOL Multiphysics, Stockholm, Sweden).

Submitted May 29, 2009, and accepted for publication July 13, 2009.

*Correspondence: lapidus@pa.msu.edu

Editor: Heinrich Roder.

0006-3495/09/09/1772/6 $2.00

doi: 10.1016/j.bpj.2009.07.003

Fluorescence changes can be observed at various times beyond mixing from ~8 to 1500 μs using the same confocal instrument described by Lapidus et al. (13) with a new charge-coupled device camera (iDus 420A-BU; Andor Technology, South Windsor, CT) that has significantly improved quantum efficiency in the UV. The temperature of the mixing chip and all solutions is raised or lowered by an aluminum manifold in contact with two thermoelectric devices (CH-77-1.0-0.8; TE Technology, Traverse City, MI) and controlled to within 0.005°C by a temperature controller (model 1600; TE Technology). The aluminum manifold was anodized and coated with parylene to prevent dissolution of aluminum salts by the buffered solutions. The mixing time can be measured by fluorescence quenching of *N*-acetyltryptophan amide (NATA) by 400 mM KI (see *inset* to Fig. 2 *c*) and is 8 μs for a flow rate of 1 m/s as calculated by a previously described method (12).

One-dimensional (1D), free-energy surface projections were calculated using the method described by Naganathan et al. (14). Briefly, this phenomenological model uses nativeness (the probability of finding a residue in native conformation) as the reaction coordinate. The conformational entropy functional (ΔS_{conf}) arises from a simple mix of native and nonnative microcanonical ensembles, whereas the stabilization energy (ΔH) is assumed to decay exponentially along the reaction coordinate. The magnitude of the exponent to the stabilization energy ($\kappa_{\Delta H}$) determines the barrier height to folding. The heat capacity functional (ΔC_p) that accounts for solvation effects is assumed to have the same curvature as the energy ($\kappa_{\Delta Cp} = \kappa_{\Delta H}$). The three functionals (entropy, energy, and heat capacity) all scale with protein size (N), and the final free-energy surface at every temperature T is calculated directly from the Gibbs-Helmholtz relation. The relaxation rates on these free-energy surfaces were computed using the matrix method of diffusive kinetics described by Lapidus et al. (15) assuming a temperature-dependent diffusion coefficient given by $D_{eff} = (k_0/N)\exp((-E_{a,res}N/R)(1/T - 1/333))$, where $E_{a,res}$ is the activation energy per residue, and k_0 is a preexponent. For the analysis described below, the cost in conformational entropy per residue and the heat capacity change per residue were fixed to the empirical values of 16.5 J/(mol.K) (at 385 K) and 58 J/(mol.K), respectively (16). The final fitted parameters are the stabilization energy per residue at 385 K (= 6.5 kJ/mol), its curvature ($\kappa_{\Delta H} = 1.9$), $E_{a,res}$ (0.4 kJ/mol), and k_0 (1.8×10^5 s^{-1}). The first two fitted parameters together with the fixed empirical terms determine the thermodynamics of the system (barrier height and stability), whereas the dynamics is determined solely by the latter two fitted parameters. The kinetic relaxations after a rapid change in landscape due to T-jump or mixing were fit to either one or two exponentials.

RESULTS AND DISCUSSION

For this work we selected three mutants of the λ-repressor fragment $\lambda_{6\text{-}85}$ created by Gruebele and co-workers, as described in Table 1. These mutants span the range of thermal stabilities and folding rates observed for this protein (8). One of these mutants (mutant 5) has been shown to exhibit biphasic unfolding kinetics, an ''activated'' rate that reflects transition over a small free-energy barrier and a ''molecular'' rate that reflects diffusion on a rough energy landscape without a significant barrier (17). It has also been the subject of numerous computational studies (14,18–20).

Equilibrium fluorescence spectra for all three mutants were recorded at temperatures between 278 and 363 K, and the equilibrium folding transition determined by both total intensity and wavelength maximum of the spectral peak. Because the quantum yield of tryptophan fluorescence has a strong intrinsic temperature dependence, the total intensity between 300 and 450 nm was normalized by a measurement of NATA at the same temperature. Fig. 1 shows these two signals scaled on different axes for mutant 5. The midpoint temperatures for each signal for all three mutants are given in Table 1. Although the T_m values for both fluorescence probes are quite close for all three mutants, there is a significant discrepancy with T_m measured by Yang and Gruebele by circular dichroism (CD) for mutants 4 and 5 (8).

Folding was observed after mixing by two methods: 1), the total intensity of light between 300 and 400 nm was recorded (Fig. 2 *a*) at various times after mixing and normalized by the same sample mixed into 6 M GdnHCl to correct for optical effects due to defects in the chip or diffusional broadening of the jet (Fig. 2 *c*); and 2), the fluorescence spectrum between 300 and 450 nm was recorded (Fig. 2 *b*) and spectra were globally analyzed using singular value decomposition (SVD). The first SVD component (*black lines* in Fig. 2, *d* and *e*) represents the average fluorescence spectrum over all times and exhibits kinetics similar to that measured by method 1, but it is not well normalized for optical or chip effects and therefore is not used. The second SVD component (*red lines* in Fig. 2, *d* and *e*) represents the spectral shift to lower wavelengths as folding progresses.

There is considerable complexity in the trends of the folding kinetics for each mutant, but we can summarize the observations with the following points:

1. For all mutants at all temperatures, the kinetics can be fit to one or two exponential decays (Fig. 2, *c* and *e*).
2. No decays require a fit to a stretched exponential.
3. The faster of the two decays has a lifetime on the order of the mixing time, and the slower of the two decays has a lifetime on the 10–100 μs timescale.
4. The amplitude of the fast phase varies from mutant to mutant, with the highest-stability protein (mutant 5) containing the least signal for the fast phase (see Fig. 5 *a*; this

TABLE 1 Equilibrium and kinetic parameters of folding

Name	Mutations	T_m* (K) (CD)	T_m† (K) (I_{total})	T_m§ (K) (λ)	ΔE_a¶ (kJ/mol) (I_{total})	ΔE_a‖ (kJ/mol) (λ)
3	Y22W A37G A49G	320.6	323.4 ± 1.7	323.0 ± 2.3	32.8	32.2
4	Y22W Q33Y A37G A49G	327.6	321.8 ± 0.5	321.7 ± 1.5	24.0	47.6
5	D14A Y22W Q33Y G46A G48A	346.6	335.8 ± 0.8	339.6 ± 2.4	18.0	45.3

*Determined by CD (8).
†Determined by total fluorescence intensity normalized by the total intensity of NATA.
§Determined by wavelength of maximum fluorescence intensity.
¶Determined by total fluorescence change after mixing.
‖Determined by second SVD component of fluorescence spectra after mixing.

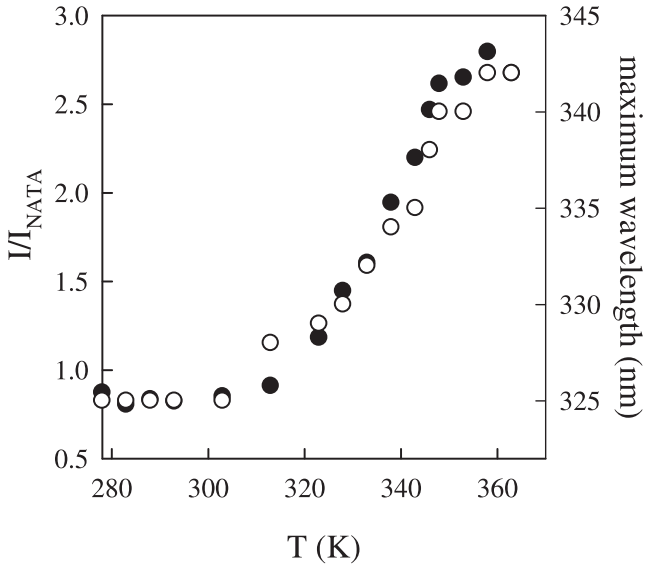

FIGURE 1 Equilibrium folding of mutant 5 as measured by total tryptophan emission, normalized by emission of NATA (*black points*) and wavelength of the maximum emission (*white points*) at various temperatures.

trend is contrary to that observed in T-jump experiments on this and other proteins in which the most stable mutants had the largest ''molecular rate'', which is due to diffusion on a rough landscape and is only observable in cases of low or no free-energy barriers (5,17)).

5. When observed by total intensity, the relative amplitude of the fast phase increases with temperature, but is fairly constant when observed by spectral shift.
6. Mutant 5 exhibits no fast phase at all as observed by spectral shift, except at the highest temperature measured (303 K; see Fig. S1 in the Supporting Material).

The rate of the slower decay is plotted as a function of $1/T$ in Fig. 3 for all three mutants. Over the range of temperatures we measured, all three mutants display Arrhenius-type kinetics, with mutants 3 and 4 showing a turnover in rate at ~10°C. This reflects a transition to the cold denatured state first described by Yang and Gruebele (21) for mutant 3. The linear portions of the curves can be fit to $k_f = k_m \exp(-\Delta E_a/RT)$, where ΔE_a is given in Table 1. For mutant 3, the rates for the spectral shift and the total intensity, as well as those measured by Yang and Gruebele (8) for the change in the Trp fluorescence lifetime, are in reasonable agreement with each other. However, there is no agreement in rates or activation energies for any of the probes used for mutants 4 and 5. These mutants show a qualitative similarity in the temperature dependence of rates for the total intensity and spectral shift. Extrapolation of the spectral shift rates for mutant 5 to ~333 K agrees with the fast ''molecular rate'' observed by Yang and Gruebele (17) (*diamonds* with *points* in Fig. 3 *c*).

Thus it appears that under the conditions observed in the mixer (low denaturant and low temperature), the folding of mutants 4 and 5 appears to involve different processes for different probes. We conclude that this is because the barrier between the folded and unfolded states is sufficiently low that different probes are sensitive to different features of the free-energy landscape. This raises the question of why mutant 3 does not exhibit this divergence. One possible answer is that the barrier for mutant 3 is sufficiently large that all probes report the same dynamics. This explanation is substantiated by the fact that mutant 3 exhibits very little difference in T_m as measured by fluorescence and CD, and is consistent with earlier results showing that a probe-dependent T_m is a sensitive indicator of the approach to the downhill folding regime (6,14,22,23). Furthermore, all three mutants follow a trend in which the divergence between the intensity and spectral shift rates decreases with decreasing thermal stability. Another explanation is that the various probes are more colocalized on the landscape than they are for mutants 4 and 5. The mutation shared by mutants 4 and 5, but not by mutant 3, is Q33Y. This mutation, which is in close contact with W22 in the folded state, may change either the order in which native contacts are made or the sensitivity of the various folding signals to particular steps in the folding path.

One way to interpret the differences in observed folding rates and equilibrium behavior is to employ a model such as that developed by Naganathan et al. (14), in which folding proceeds by diffusion on a 1D, free-energy surface. Under this assumption, if there is only a small free-energy barrier between the unfolded and folded states, then the observed rates and equilibrium T_m will reflect the exact location of the folding signatures on the reaction coordinate (Fig. 4 *a*). Thus the spectral shift is sensitive to population redistributions far from the native state, whereas the total intensity and fluorescence lifetime are sensitive close to the native state. Note that this ordering is in agreement with the general assumption that hydrophobic collapse precedes the formation of native contacts. An analysis was performed to match all the available data for mutant 5, and the results are shown in Fig. 4. Fig. 4 *a* shows that as the temperature decreases, the free-energy surface becomes downhill, with a significant increase in free energy of the least-native conformations. These two features correspond to two of the building blocks of free-energy landscapes described by Liu and Gruebele (24) that lead to multiexponential and probe-dependent kinetics. The predicted barrier at $T = 338$ K is ~2 kJ/mol, which is slightly lower than that estimated by Yang and Gruebele (3).

The equilibrium signal change is plotted in Fig. 4 *d* and predicts a slightly lower T_m for the total intensity change (~336 K) compared to the spectral shift (~341 K) because a switch closer to the unfolded basin will have a higher apparent stability than one closer to the native basin, in agreement with the measured T_m in Table 1. Assuming the unfolded free-energy surface in 6 M GdnHCl resembles that at 373 K, we calculated the relaxation after jumping from this surface (*continuous black curve* in Fig. 4 *a*) to those at various experimental temperatures. The model predicts quasi-perfect single exponential decays (Fig. S2) at all

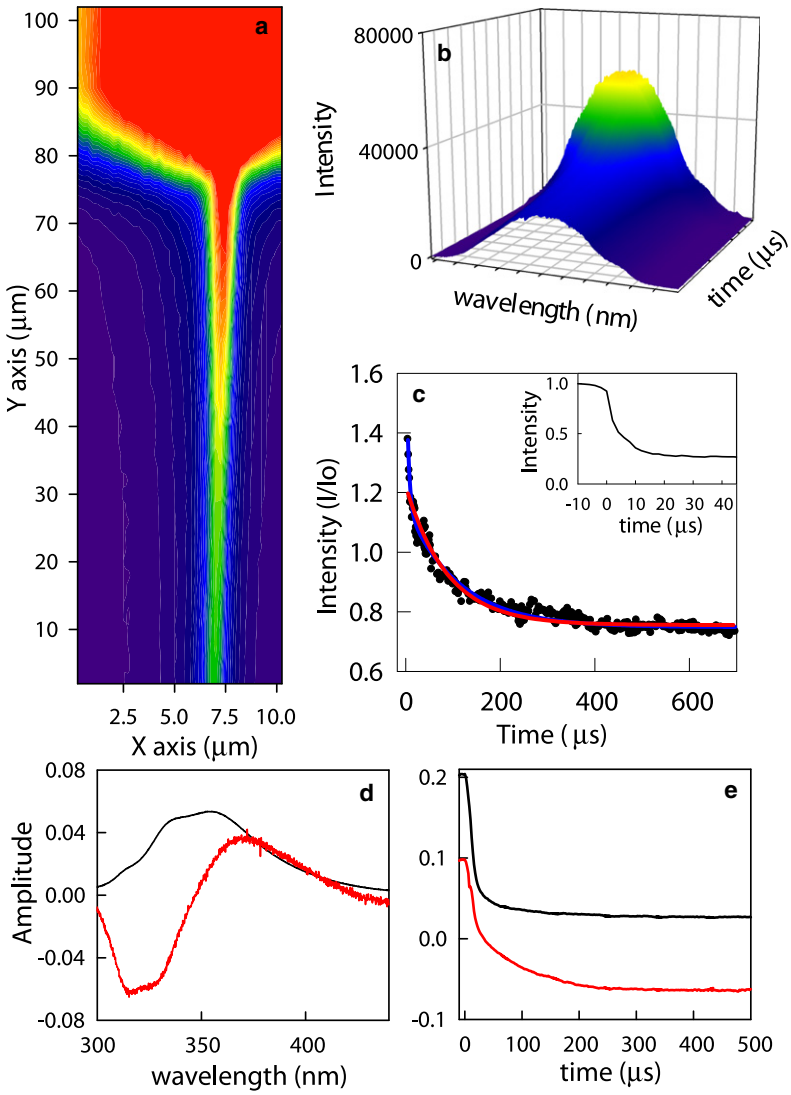

FIGURE 2 (*a*) Fluorescence changes observed in the microfluidic mixer. The fluorescent protein in 6 M GdnHCl flows down from the top of the graph and is mixed with 100 mM phosphate buffer at a 100-fold higher flow rate, diluting the denaturant and constricting the protein to a narrow jet. Then the protein proceeds to fold, further decreasing fluorescence. (*b*) Fluorescent spectra observed along the jet plotted versus time. (*c*) The relative intensity (compared to mixing the protein into 6 M GdnHCl) over 1.25 × 2 μm areas of the jet is plotted as a function of time for two linear flow rates of 1.64 and 0.66 m/s. The sample is mutant 4 at 313 K. The lines are fits to one exponential (k_1 = 11408 s^{-1}; *red*) and two exponentials (k_1 = 9110 s^{-1}, k_2 = 205,987 s^{-1}; *blue*). (*Inset*) The relative intensity of NATA mixed into 400 mM KI shows the mixing time for a flow rate of 1 m/s. (*d*) The two most significant SVD components of the time-resolved spectra representing the average (*black*) and difference (*red*) spectra. The sample is mutant 4 at 293 K. The singular values of these components are 1.0 × 10^6 (*black*) and 7.5 × 10^4 (*red*). (*e*) SVD amplitudes versus time.

temperatures for both probes with rates that agree well with the measured rates (*dark gray circles* and *line* and *light gray triangles* and *line* in Fig. 4 *c*).

The free-energy surfaces predicted by this model also reproduce the relaxation after T-jump of the tryptophan fluorescence lifetime as measured by Yang and Gruebele (8). These experiments were performed at temperatures at which there is a marginal barrier (~2 kJ/mol). Assuming this probe follows a signature switch near the barrier (*black line* in Fig. 4 *a*), these relaxations exhibit biexponential kinetics as populations on either side of the barrier redistribute (Fig. S2). Although the predicted relative amplitudes of these two phases agree with experiment (Fig. 4 *e*), the predicted rates are in slight disagreement with the observed rates (Fig. 4 *c*). This discrepancy could be due to the large uncertainty in fitting two exponentials with time constants that

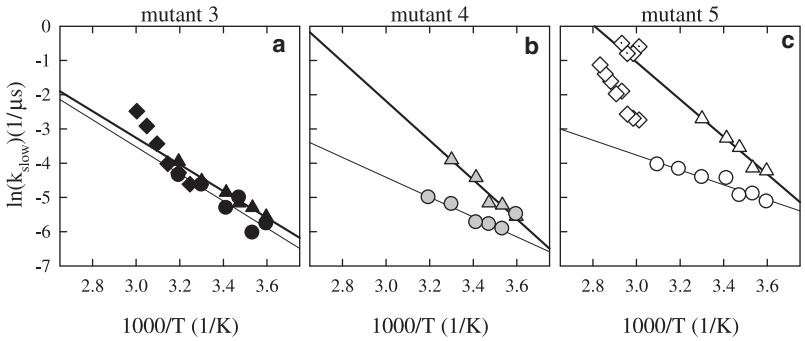

FIGURE 3 Slower rates observed by tryptophan fluorescence intensity (*circles*), spectral shift (*triangles*), and lifetime (*diamonds*, observed by Yang and Gruebele (8)) for mutants 3 (*a*), 4 (*b*), and 5 (*c*). The rates in this work come from two exponential fits in which one of the rates is >10^5 s^{-1}. If there is no obvious decay on that timescale, the fit was constrained to a single exponential. Lines are fits to $k_f = k_m \exp(-\Delta E_a/kT)$, where ΔE_a is given in Table 1, with the thick line fitting the spectral shift rates and the thin line fitting the intensity rates. The accuracy of each rate is ~10% and the accuracy of each temperature is 0.2°C.

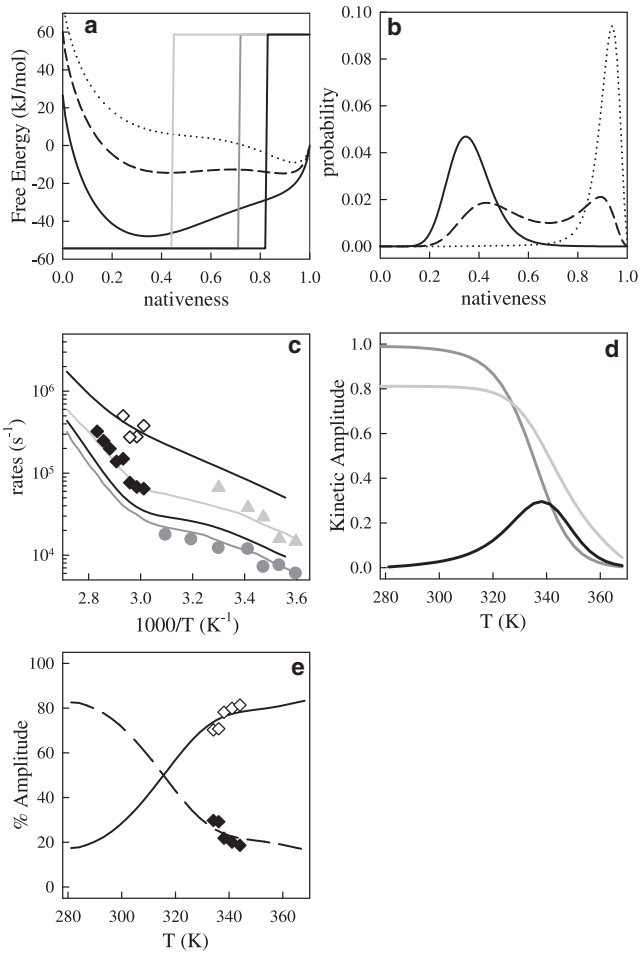

FIGURE 4 (*a*) Free-energy surfaces used to model the experimental data for mutant 5 at T = 298 K (*dotted*), 338 K (*dashed*), and 373 K (*solid*). The straight lines are the signal switches for the various probes. In all panels, the light gray, dark gray and black correspond to the tryptophan spectral shift, intensity change, and lifetime, respectively. (*b*) Equilibrium probability distributions of number of native contacts at the same temperatures shown in *a*. (*c*) Exponential rates predicted (*lines*) and measured (*symbols*) by all signals. The gray lines correspond to relaxation rates after jumping from 373 K, and the black lines correspond to rates after jumping up in temperature 10 K. The points are the same data plotted in Fig. 3 *c* using the same symbols. (*d*) Kinetic amplitude versus temperature for all three probes. The midpoint of the gray curves and the peak of the black curve are the apparent melting temperatures for these signals. (*e*) Predicted (*lines*) and measured (*points*) relative amplitudes of the faster (*black points* and *dashed line*) and slower (*white points* and *solid line*) rates observed after T-jump.

vary by a factor of <5 (M. Gruebele, University of Illinois, personal communication, 2008).

The kinetic results together with the equilibrium differences in T_m strongly support downhill folding behavior in mutant 5. The folding diffusion coefficients at low temperatures (<300 K) can be as slow as 10,000–20,000 s^{-1}, in agreement with previous empirical (14) and experimental estimates (4) while being consistent with faster experimental measurements at higher temperatures (3). A much larger free-energy barrier fails to reproduce differences in rates or melting temperatures for the two probes. Therefore, from this analysis we conclude that the observed dynamics at low temperatures are downhill diffusive relaxations.

A similar analysis of mutant 3 shows that the relaxation rates and T_m can be probe-independent with a larger barrier (6 kJ/mol at T_m = 323 K) than that for mutant 5 and if all the signal switches are colocalized (Fig. S3). For the switches to be the same as for mutant 5 (Fig. 4 *a*), the barrier for mutant 3 at the thermal midpoint must be ~8 kJ/mol, but this leads to clear biexponential kinetics at all temperatures. Therefore, it seems likely that the mutational differences between mutant 3 and mutants 4 and 5 both raise the barrier between the folded and unfolded basins and change the folding path.

Although a 1D free-energy surface does an adequate job of explaining kinetic and equilibrium observations, we cannot strictly rule out the existence of multiple reaction coordinates. Hagen (25) has shown that 2D landscapes with barriers can produce the nonexponential, probe-dependent kinetics often attributed to 1D downhill folding paths, although that model cannot quantitatively explain mutational and solvent effects in λ (26). Indeed, there is evidence that the submicrosecond kinetics do not conform to a 1D potential. The relaxation that occurs during mixing cannot be resolved and is faster than 2×10^5 s^{-1} even for the lowest temperatures measured. However, the amplitude of the fast phase can be estimated from the difference between the total intensity change and the amplitude of the slow decay (Fig. 5). As the absolute amplitude of the slow phase decreases as the temperature (Fig. 5 *a*) or GdnHCl (Fig. 5 *b*) increases, the amplitude of the fast phase remains relatively constant, leading to a relative decrease in the slow phase. This suggests that the fast process is a relaxation in the unfolded state that is even faster than that observed by the spectral shift switch. Indeed, placement of a switch anywhere on the surface in Fig. 4 *a* cannot produce submicrosecond kinetics at low temperatures without the use of a larger diffusion coefficient, which would be too large to account for the slower rates. This process may be the same as that observed by Dumont et al. (27) in a <5 ms burst phase detected by CD at low temperature and high viscosity in two other mutants of $\lambda_{6\text{-}85}$, but the timescales and temperatures are too disparate to make a quantitative comparison. The timescale of this phase is commensurate with hydrophobic collapse as observed in BBL, cytochrome *c*, apomyogolobin, lysozyme, and protein L (13,28,29), so we assume this is the same process in λ. Using a 1D globally downhill surface for BBL, Li et al. (4) concluded that the observed fast collapse must progress along a reaction coordinate orthogonal to nativeness. This may be true as well for λ, but our inability to fully resolve this process prevents unequivocal assignment to a particular coordinate. Furthermore, measurements of intramolecular diffusion in protein L and protein G show that it slows down dramatically upon dilution of the denaturant (30), so the effective ''roughness'' of the landscape will change during mixing. Nevertheless, the fact that a submicrosecond

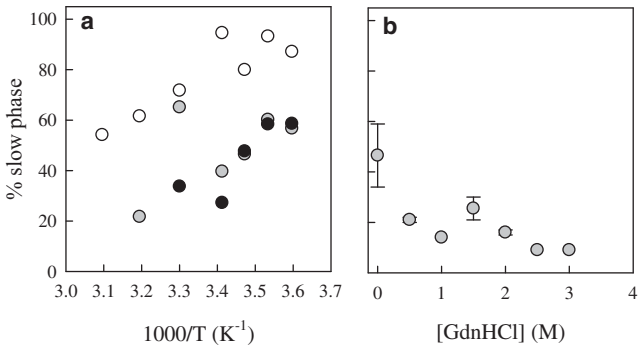

FIGURE 5 Relative amplitude of the slower phase (rates shown in Fig. 3) after mixing as observed by total fluorescence mutants 3 (*black*), 4 (*gray*), and 5 (*white*) versus temperature (*a*) and denaturant concentration (*b*).

phase was never observed by T-jump suggests that unfolded states accessed by high temperature and 6 M GdnHCl are not the same, supporting the requirement of a multidimensional landscape.

SUPPORTING MATERIAL

Three figures are available at http://www.biophysj.org/biophysj/supplemental/S0006-3495(09)01223-5.

The authors thank Martin Gruebele for the kind gift of protein and plasmids, and for many enlightening discussions.

This work was supported by funding from the National Science Foundation (NSF) Frontiers in Integrative Biological Research Program (grant EF-0623664) and administered in part by the Center for Biophotonics, an NSF Science and Technology Center, managed by the University of California, Davis, under Cooperative Agreement PHY 0120999. The research of Lisa Lapidus, PhD, was supported in part by a Career Award at the Scientific Interface from the Burroughs Wellcome Fund. Work at Lawrence Livermore National Laboratory was performed under the auspices of the U.S. Department of Energy under contract DE-AC52-07NA27344 with funding from the Laboratory Directed Research and Development Program.

REFERENCES

1. Socci, N. D., J. N. Onuchic, and P. G. Wolynes. 1996. Diffusive dynamics of the reaction coordinate for protein folding funnels. *J. Chem. Phys.* 104:5860–5868.
2. Bryngelson, J. D., J. N. Onuchic, N. D. Socci, and P. G. Wolynes. 1995. Funnels, pathways, and the energy landscape of protein-folding—a synthesis. *Proteins*. 21:167–195.
3. Yang, W. Y., and M. Gruebele. 2003. Folding at the speed limit. *Nature*. 423:193–197.
4. Li, P., F. Y. Oliva, A. N. Naganathan, and V. Munoz. 2009. Dynamics of one-state downhill protein folding. *Proc. Natl. Acad. Sci. USA*. 106:103–108.
5. Liu, F., D. G. Du, A. A. Fuller, J. E. Davoren, P. Wipf, et al. 2008. An experimental survey of the transition between two-state and downhill protein folding scenarios. *Proc. Natl. Acad. Sci. USA*. 105:2369–2374.
6. Liu, F., and M. Gruebele. 2007. Tuning λ(6–85) towards downhill folding at its melting temperature. *J. Mol. Biol.* 370:574–584.
7. Ma, H. R., and M. Gruebele. 2005. Kinetics are probe-dependent during downhill folding of an engineered λ (6–85) protein. *Proc. Natl. Acad. Sci. USA*. 102:2283–2287.
8. Yang, W. Y., and M. Gruebele. 2004. Rate-temperature relationships in λ-repressor fragment λ (6–85) folding. *Biochemistry*. 43:13018–13025.
9. Knight, J. B., A. Vishwanath, J. P. Brody, and R. H. Austin. 1998. Hydrodynamic focusing on a silicon chip: mixing nanoliters in microseconds. *Phys. Rev. Lett.* 80:3863–3866.
10. Hertzog, D. E., B. Ivorra, B. Mohammadi, O. Bakajin, and J. G. Santiago. 2006. Optimization of a microfluidic mixer for studying protein folding kinetics. *Anal. Chem.* 78:4299–4306.
11. Hertzog, D. E., X. Michalet, M. Jager, X. X. Kong, J. G. Santiago, et al. 2004. Femtomole mixer for microsecond kinetic studies of protein folding. *Anal. Chem.* 76:7169–7178.
12. Yao, S., and O. Bakajin. 2007. Improvements in mixing time and mixing uniformity in devices designed for studies of protein folding kinetics. *Anal. Chem.* 79:5753–5759.
13. Lapidus, L. J., S. Yao, K. S. McGarrity, D. E. Hertzog, E. Tubman, et al. 2007. Protein hydrophobic collapse and early folding steps observed in a microfluidic mixer. *Biophys. J.* 93:218–224.
14. Naganathan, A. N., U. Doshi, and V. Munoz. 2007. Protein folding kinetics: barrier effects in chemical and thermal denaturation experiments. *J. Am. Chem. Soc.* 129:5673–5682.
15. Lapidus, L. J., P. J. Steinbach, W. A. Eaton, A. Szabo, and J. Hofrichter. 2002. Effects of chain stiffness on the dynamics of loop formation in polypeptides. Appendix: testing a 1-dimensional diffusion model for peptide dynamics. *J. Phys. Chem. B*. 106:11628–11640.
16. Robertson, A. D., and K. P. Murphy. 1997. Protein structure and the energetics of protein stability. *Chem. Rev.* 97:1251–1268.
17. Yang, W. Y., and M. Gruebele. 2004. Folding λ-repressor at its speed limit. *Biophys. J.* 87:596–608.
18. Larios, E., J. W. Pitera, W. C. Swope, and M. Gruebele. 2006. Correlation of early orientational ordering of engineered λ (6–85) structure with kinetics and thermodynamics. *Chem. Phys.* 323:45–53.
19. Qi, X., and J. J. Portman. 2007. Excluded volume, local structural cooperativity, and the polymer physics of protein folding rates. *Proc. Natl. Acad. Sci. USA*. 104:10841–10846.
20. Shen, T. Y., C. H. Zong, J. J. Portman, and P. G. Wolynes. 2008. Variationally determined free energy profiles for structural models of proteins: characteristic temperatures for folding and trapping. *J. Phys. Chem. B*. 112:6074–6082.
21. Yang, W. Y., and M. Gruebele. 2005. Kinetic equivalence of the heat and cold structural transitions of λ (6–85). *Phil. Trans. R. Soc. Lond.* 363:565–573.
22. Sadqi, M., D. Fushman, and V. Muñoz. 2006. Atom-by-atom analysis of global downhill protein folding. *Nature*. 442:317–321.
23. Garcia-Mira, M. M., M. Sadqi, N. Fischer, J. M. Sanchez-Ruiz, and V. Muñoz. 2002. Experimental identification of downhill protein folding. *Science*. 298:2191–2195.
24. Liu, F., and M. Gruebele. 2008. Downhill dynamics and the molecular rate of protein folding. *Chem. Phys. Lett.* 461:1–8.
25. Hagen, S. J. 2007. Probe-dependent and nonexponential relaxation kinetics: unreliable signatures of downhill protein folding. *Proteins*. 68:205–217.
26. Gruebele, M. 2008. Comment on probe-dependent and nonexponential relaxation kinetics: unreliable signatures of downhill protein folding. *Proteins*. 70:1099–1102.
27. Dumont, C., Y. Matsumura, S. J. Kim, J. S. Li, E. Kondrashkina, et al. 2006. Solvent-tuning the collapse and helix formation time scales of λ (*)(6–85). *Protein Sci.* 15:2596–2604.
28. Sadqi, M., L. J. Lapidus, and V. Munoz. 2003. How fast is protein hydrophobic collapse? *Proc. Natl. Acad. Sci. USA*. 100:12117–12122.
29. Waldauer, S. A., O. Bakajin, T. Ball, Y. Chen, S. J. DeCamp, et al. 2008. Ruggedness in the folding landscape of protein L. *HFSP J.* 2:388–395.
30. Singh, V. R., M. Kopka, Y. Chen, W. J. Wedemeyer, and L. J. Lapidus. 2007. Dynamic similarity of the unfolded states of proteins L and G. *Biochemistry*. 46:10046–10054.